Article

Improvement of H₂S Sensing Properties of SnO₂-Based Thick Film Gas Sensors Promoted with MoO₃ and NiO

Soo Chool Lee [1,†], Seong Yeol Kim [1,†], Byung Wook Hwang [1], Suk Yong Jung [1], Dhanusuraman Ragupathy [2], In Sung Son [3], Duk Dong Lee [4] and Jae Chang Kim [1,*]

[1] Department of Chemical Engineering, Kyungpook National University, Daegu 702-701, Korea;
E-Mails: soochool@knu.ac.kr (S.C.L.); ksy228@nate.com (S.Y.K.); a048042@knu.ac.kr (B.W.H.);
ojhyt@hanmail.net (S.Y.J.)

[2] Centre for Research & Development, PRIST University, Puducherry 605 007, India;
E-Mail: ragupathypdy@prist.ac.in

[3] HKC, Sucho-gu, Seoul 130-070, Korea; E-Mail: HKC1959@hkc.co.kr

[4] School of Electrical Engineering and Computer Science, Kyungpook National University,
Daegu 702-701, Korea; E-Mail: ddlee@knu.ac.kr

[†] These authors contributed equally to this work.

[*] Author to whom correspondence should be addressed; E-Mail: kjchang@knu.ac.kr;
Tel.: +82-53-950-5622; Fax: +82-53-950-6615.

Abstract: The effects of the SnO₂ pore size and metal oxide promoters on the sensing properties of SnO₂-based thick film gas sensors were investigated to improve the detection of very low H₂S concentrations (<1 ppm). SnO₂ sensors and SnO₂-based thick-film gas sensors promoted with NiO, ZnO, MoO₃, CuO or Fe₂O₃ were prepared, and their sensing properties were examined in a flow system. The SnO₂ materials were prepared by calcining SnO₂ at 600, 800, 1,000 and 1,200 °C to give materials identified as SnO₂(600), SnO₂(800), SnO₂(1000), and SnO₂(1200), respectively. The Sn(12)Mo5Ni3 sensor, which was prepared by physically mixing 5 wt% MoO₃ (Mo5), 3 wt% NiO (Ni3) and SnO₂(1200) with a large pore size of 312 nm, exhibited a high sensor response of approximately 75% for the detection of 1 ppm H₂S at 350 °C with excellent recovery properties. Unlike the SnO₂ sensors, its response was maintained during multiple cycles without deactivation. This was attributed to the promoter effect of MoO₃. In particular, the Sn(12)Mo5Ni3 sensor developed in this study showed twice the response of the Sn(6)Mo5Ni3 sensor,

which was prepared by $SnO_2(600)$ with the smaller pore size than $SnO_2(1200)$. The excellent sensor response and recovery properties of Sn(12)Mo5Ni3 are believed to be due to the combined promoter effects of MoO_3 and NiO and the diffusion effect of H_2S as a result of the large pore size of SnO_2.

Keywords: sensor; SnO_2; pore size; H_2S; MoO_3; NiO

1. Introduction

Hydrogen sulfide (H_2S) is an unwanted and toxic by-product of the coal, coal oil, and natural gas industries [1]. When hydrogen sulfide is emitted into the atmosphere, it is converted to SO_x, which is a precursor to acid rain [2]. Accordingly, there is increasing demand for sensing devices that monitor low H_2S concentrations. Well-known materials used to detect H_2S include $BaTiO_3$ [3], SnO_2-Pd [4], Ag-SnO_2 [5], SnO_2-Al_2O_3 [6], SnO_2-CuO [7–11], SnO_2-CuO-SnO_2 [12,13], SnO_2-ZnO-CuO [14] and SiO_2-doped Cu-Au-SnO_2 [15]. Among the sensors described in the literature, CuO-modified thin-film or thick-film SnO_2 sensors are promising for the sensitive and selective detection of H_2S [1].

SnO_2-based thick-film gas sensors have been used to detect toxic gases [16–28] on account of their high sensor response, simple design, low weight and low price. SnO_2-based thick film gas sensors can achieve greater sensitivity to H_2S through control of the particle size [17] and the addition of suitable promoters [13,14]. Wagh *et al*. reported that SnO_2-ZnO-CuO thick-film sensors had significantly better response and recovery times than SnO_2-ZnO or CuO doped SnO_2 sensors [15]. Nevertheless, most studies on the sensing behavior of CuO-modified SnO_2 thick-film gas sensors focused on concentrations of tens to hundreds of ppm. Until now, there have been very few studies of SnO_2-based gas thick-film sensors for the detection of <1 ppm H_2S.

In our previous papers, we described a SnO_2-based thick-film gas sensor promoted with MoO_3 and NiO, which was developed for the detection of dimethyl methylphosphonate (DMMP) and dichloromethane [26–28]. During the course of this earlier study, NiO and MoO_3 promoters were found to play important roles in the sensor response and the recovery of the SnO_2-based sensor, respectively, for the detection of toxic organic compounds containing P and Cl [26–28]. In the case of H_2S detection, a SnO_2-based thick-film sensor promoted with NiO and MoO_3 showed improved recovery properties [2]. Nevertheless, the response of this sensor was decreased by promoting MoO_3 despite the good recovery properties. Considering that the sensor response is an important factor in addition to the recovery properties, the improvement in the sensor response is necessary to develop a new SnO_2-based thick-film gas sensor for the detection of <1 ppm H_2S.

The aim of this study was to improve the response of a SnO_2-based thick-film gas sensor promoted with NiO and MoO_3 developed in a previous study for the detection of H_2S at concentrations of <1 ppm. Accordingly, this study examined the effects of promoters and the textural properties of SnO_2 on the sensing behaviors of SnO_2-based thick-film sensors.

2. Experimental Section

2.1. Preparation of the Materials and Sensors

The SnO_2 used as a source for the SnO_2-based sensors was prepared from $SnCl_4$ using a previously described ammonia-based precipitation method [2,26–28]. The products were calcined in a muffle furnace at various temperatures (600, 800, 1,000 or 1,200 °C). The SnO_2-based materials were prepared by physically mixing two or three of the following promoters, NiO, ZnO, MoO_3, CuO and Fe_2O_3, with SnO_2. All products were calcined in a muffle furnace at 600 °C for 4 hours. The temperature ramp rate was 3 °C/min. The thick–film sensors were fabricated on an alumina substrate by screen-printing using a variety of physical mixtures, such as a SnO_2-based powder and an organic binder (90% α-terpineol, Aldrich) [2,26–28]. The printed thick-film sensors were dried and calcined at 600 °C for 1 hour. This paper describes the sensors as $SnO_2(600)$ or Sn(6)Mo5Ni3, where (600) represents the calcination temperature, Sn(6) represents SnO_2 calcined at 600 °C, Mn5 and Ni3 represent 5% MoO_3 and 3% NiO, respectively, on a weight/weight basis.

2.2. Sensor Testing System

The sensing behaviors were examined in a flow system equipped with a 0.1 L chamber. The H_2S gas was diluted with dry air to a concentration of <4.0 ppm. The total flow rate of the gas mixture was 400 mL/min. H_2S gas was injected into chamber for 10 minutes. In the present study, the sensor response was defined using the following equation:

$$\text{Sensor response (\%)} = [(R_a - R_g)/R_a] \times 100 \qquad (1)$$

where R_a and R_g are the electric resistance in air and test gas, respectively. The sensor recovery was defined by the following equation:

$$\text{Recovery (\%)} = [(S_m - S_r)/S_m] \times 100 \qquad (2)$$

where S_m and S_r represent the maximum sensor response over a period of 10 minutes and the minimum sensor response in air, respectively.
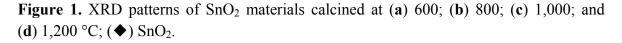
2.3. Characterization of Materials

The crystalline phases in the materials were identified by power X-ray diffraction (XRD; Philips, X'PERT) using Cu Kα radiation. The morphology of the SnO_2 powder was observed by transmission electron microscopy (TEM; Hitachi, H-7100), and the textural properties of the materials were examined using an Hg porosimetry (Micromeritics, AutoPore IV 9500).
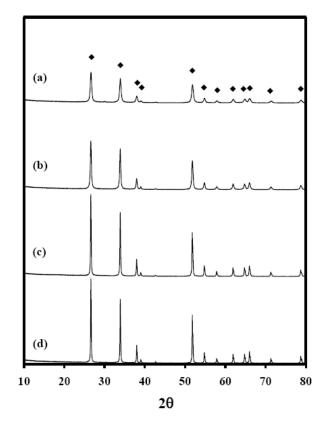
3. Results and Discussion

3.1. Effects of SnO_2 Pore Size on Sensor Properties

To examine the effects of the textural properties of SnO_2 on the sensing properties, the SnO_2 materials were prepared by calcining SnO_2 at temperatures of 600, 800, 1000, and 1,200 °C

[affording materials identified as $SnO_2(600)$, $SnO_2(800)$, $SnO_2(1000)$, and $SnO_2(1200)$, respectively]. Figure 1 shows XRD patterns of the SnO_2 materials.

Figure 1. XRD patterns of SnO_2 materials calcined at (**a**) 600; (**b**) 800; (**c**) 1,000; and (**d**) 1,200 °C; (◆) SnO_2.

Diffraction peaks were observed at 26.6, 33.8, 37.9, 51.8, 54.8, 61.9, 64.7, 65.9 and 71.3° 2θ, and the intensities of these diffraction peaks increased with increasing temperature, indicating an increase in the crystallite size and the crystallinity [29,30], but the structures of SnO_2 were retained. To confirm these results, the sizes of the SnO_2 crystallites were calculated from the XRD patterns using Scherrer's equation Equation (3). As expected, the crystallite size of SnO_2 increased from 19 to 54 nm with increasing calcination temperature (Table 1).

$$t = (K \cdot \lambda)/(W_{size} \cdot \cos\theta) = (0.9 \cdot \lambda)/(FWHM \cdot \cos\theta) \tag{3}$$

Table 1. Crystallite sizes calculated using XRD and TEM data.

| SnO₂ materials | XRD | | | | TEM |
	Wave Length (nm)	2θ (°)	FWHM (cm³/g)	Crystallite Size (nm)	Crystallite Size (nm)
$SnO_2(600)$	0.154	26.611	0.4095	19	10–20
$SnO_2(800)$	0.154	26.581	0.3104	26	25–30
$SnO_2(1,000)$	0.154	26.585	0.1690	47	40–50
$SnO_2(1,200)$	0.154	26.604	0.1488	54	50–70

In a separate experiment, TEM images of these SnO_2 materials were investigated. Table 1 lists the crystallite sizes obtained from TEM images, which concur with those determined by XRD. Table 2

lists the textural properties of SnO_2 materials, as determined by Hg porosimetry. The surface areas decreased with increasing calcination temperature, whereas the average pore diameters increased, presumably because the pore diameter is dependent on the crystallite size.

Table 2. Textural properties of the SnO_2 materials produced by Hg porosimetry.

SnO_2 Materials	Surface Area (m^2/g)	Pore Volume (cm^3/g)	Average Pore Diameter (nm)
SnO_2(600)	24.8	0.4918	79
SnO_2(800)	16.4	0.5047	122
SnO_2(1000)	9.4	0.5226	222
SnO_2(1200)	8.0	0.6263	312

Figure 2 shows the response curves, responses and 80% response times of SnO_2(600), SnO_2(800), SnO_2(1000) and SnO_2(1200) gas sensors at a H_2S concentration of 1.0 ppm at 350 °C. The responses of the SnO_2-based sensors increased in the following order: SnO_2(600) < SnO_2(800) < SnO_2(1000) < SnO_2(1200). The response time of the SnO_2(1200) sensor was much shorter than that of the SnO_2(600) sensor, even though sensor recovery was incomplete in air. These results mean that the response time decreases with increasing pore diameter, as shown in Table 1 and Figure 2(II), and the sensor response increases. However, the important point to note is the incomplete recovery of the sensors after the detection of H_2S, despite the high sensor response. It is thought that this result is because sulfur compounds are adsorbed on the sensor's surface, and that they progressively pollute the surface of tin dioxide.

Figure 2. (**I**) Response curves, (**II**) responses, and (II) 80% response times of SnO_2-based gas sensors, such as (a) SnO_2(600); (b) SnO_2(800); (c) SnO_2(1000); and (d) SnO_2(1200) at a H_2S concentration of 1.0 ppm at 350 °C.
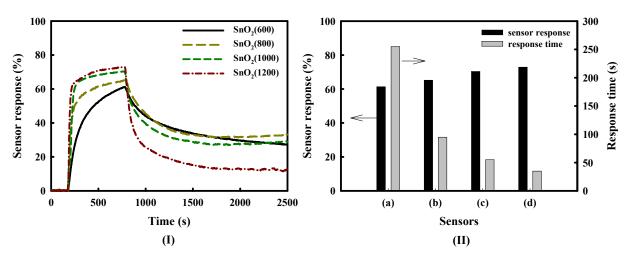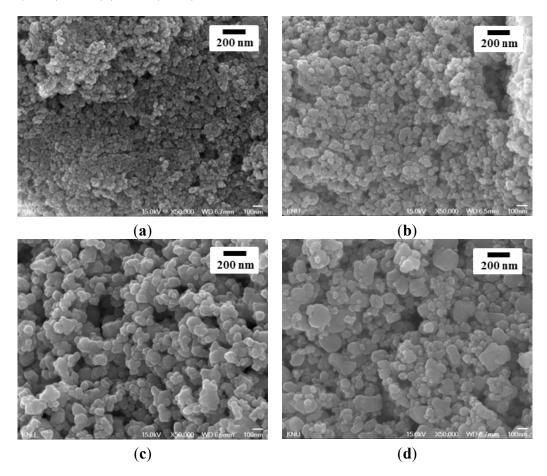

Figure 3 shows SEM images of the surfaces of the SnO_2(600), SnO_2(800), SnO_2(1000) and SnO_2(1200) thick-film sensors. The particle size of SnO_2 increased with increasing calcination temperature in the following order: SnO_2(600) < SnO_2(800) < SnO_2(1000) < SnO_2(1200). Liu *et al*. reported that the sensor sample based on SnO_2 nanocrystals produced by the gel combustion method had higher response and shorter response times, which might be due to the more porous nano-crystallinity (~50 nm in size) than the sample prepared from hydrothermal-synthesized SnO_2

nanocrystals, where smaller SnO_2 nanocrystals (~12–13 nm) are densely packed and agglomerate into large entities (secondary particles), approximately 2–3 μm in size [17]. However, in this study, particle size after screen-printing, as well as average pore diameter of SnO_2, is directly related to the crystallite size (Table 1) and the crystalinity of SnO_2, which is in contrast to Liu *et al.*'s results. This result is because the crystallite size and the crystalinity of SnO_2 was controlled by calcining the SnO_2 material, which was prepared by precipitation, at various temperatures (600, 800, 1,000 and 1,200 °C), and the SnO_2 thick–film sensors were fabricated on an alumina substrate by screen-printing using these calcined materials. From these results, it is clear that the sensor response and response time for the detection of H_2S gas are directly affected by the SnO_2 pore diameter rather than to the surface area due to the diffusion of H_2S gas. In particular, the important point to note is that the response time of the SnO_2 sensor, as well as sensor response for the detection of H_2S, can be enhanced by increasing the crystallite size of SnO_2 by calcination.

Figure 3. SEM images of the SnO_2 thick-film sensors: (**a**) SnO_2(600); (**b**) SnO_2(800); (**c**) SnO_2(1000); and (**d**) SnO_2(1200).

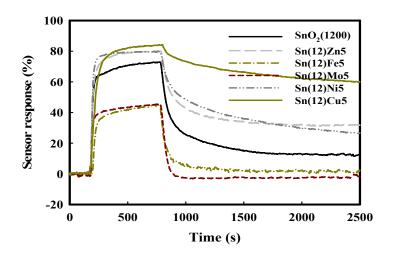(**a**)

(**b**)

(**c**)

(**d**)

3.2. Promoter Effects on Sensor Response and Recovery

The sensor recovery properties are an important consideration for sensors designed for H_2S. To improve the sensor recovery, SnO_2(1200)-based sensors were prepared by physically mixing with ZnO, Fe_2O_3, MoO_3, NiO, or CuO promoters, which are referred to as Sn(12)Zn, Sn(12)Fe5, Sn(12)Mo5, Sn(12)Ni5, and Sn(12)Cu5, respectively. The effects of the promoters on the sensor

recovery properties were investigated at a H_2S concentration of 1.0 ppm at 350 °C. The results obtained are summarized in Figure 4. The Sn(12)Zn5, Sn(12)Ni5 and Sn(12)Cu5 sensors showed a slight increase in the sensor response compared to the SnO_2 sensor, but their recoveries were incomplete at 350 °C. On the other hand, Sn(12)Fe5 and Sn(12)Mo5 showed complete recovery, but exhibited much lower responses than the $SnO_2(1200)$ sensor. In particular, the Sn(12)Mo5 sensor showed a faster recovery time than the Sn(12)Fe5 sensor, and a response that was approximately 42% higher than that of the $SnO_2(600)$-based sensor containing 5 wt% MoO_3 [Sn(6)Mo5]. The reason for excellent recovery properties of the Fe5 and Mo5 sensors is not clear yet, but it is thought that Fe_2O_3 and MoO_3 promoters added to SnO_2 play an important role in the desorption of sulfur compounds. To identify the effects of the promoters on the sensor response and recovery, the SnO_2-based sensors promoted with various amounts of metal oxides (MoO_3, NiO_3, and ZnO) were examined at 1 ppm H_2S and 350 °C. These results are shown in Figure 5. As shown by Figures 5(b,c) and (d), the Sn(12)Mo5 sensor achieved a recovery of 100%, even though the sensor response was decreased by the MoO_3 promoter. Previous studies found that NiO plays an important role in enhancing the sensor response of the SnO_2-based sensor promoted with MoO_3 for the detection of dimethyl methylphosphonate (DMMP) and dichloromethane [23,24]. In the present study, the sensor response for the detection of H_2S was increased by NiO (Figure 5). As expected, the Sn(12)Mo5Ni3 sensor, which was promoted with both MoO_3 and NiO, showed a sharp increase in the sensor response and maintained the sensor recovery properties (Figure 5(f)). In particular, the Sn(12)Mo5Ni3 sensor exhibited much higher sensor response and recovery than the Sn(6)Mo5Ni3 sensor [2] (39.2% and 91%, respectively). These results are attributed to diffusion effects caused by the larger pore size of SnO_2 and the promoter effects of NiO and MoO_3. However, further study is required to verify the sensing mechanisms and the roles of NiO, ZnO, CuO, MoO_3, and Fe_2O_3 promoters in the sensor response and recovery properties.

Figure 4. Response curves of the SnO_2-based gas sensors promoted with various metal oxides at a H_2S concentration of 1.0 ppm at 350 °C.

Figure 5. Responses and recoveries of the SnO$_2$-based gas sensors promoted with various amounts of metal oxides at a H$_2$S concentration of 1.0 ppm at 350 °C; (a) SnO$_2$(1200); (b) Sn(12)Mo1; (c) Sn(12)Mo3; (d) Sn(12)Mo5; (e) Sn(12)Mo5Ni1; (f) Sn(12)Mo5Ni3; (g) Sn(12)Mo5Ni5; (h) Sn(12)Mo5Zn3; and (i) Sn(6)Mo5Ni3.
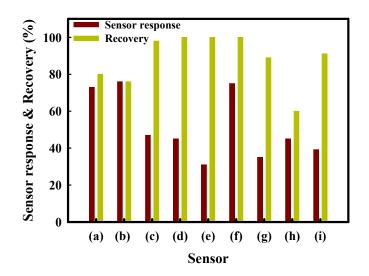

Figure 6 shows the response and recovery of the Sn(12)Mo5Ni3 sensor as a function of temperature at a H$_2$S concentration of 1.0 ppm. The sensor response decreased slightly with increasing detection temperature, whereas the sensor recovery increased between 250 °C and 350 °C. Considering the sensor response and recovery, the optimum temperature for the detection of H$_2$S was 350 °C.

Figure 6. Responses and recovery of the Sn(12)Mo5Ni3 sensor as a function of the detection temperature at a H$_2$S concentration of 1.0 ppm.
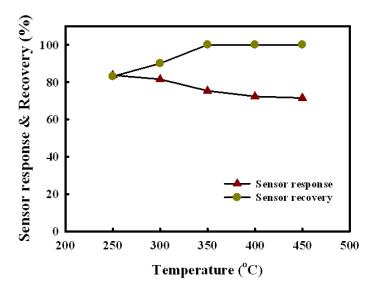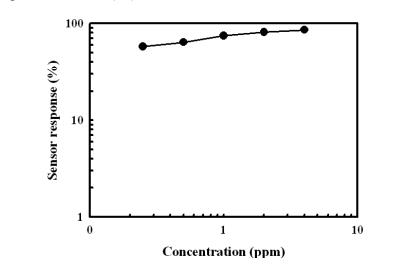

Figure 7 shows the response of the Sn(12)Mo5Ni3 sensor at concentrations between 0.25 ppm and 4 ppm at 350 °C. The response of this sensor increased almost linearly between 0.25 ppm and 4 ppm. The Sn(12)Mo5Ni3 sensor had a high sensor response of approximately 59% at low H$_2$S concentrations of 0.25 ppm.

Figure 7. Response of the Sn(12)Mo5Ni3 sensor as a function of the H$_2$S concentration.

Figure 8 shows the repeatabilities of the SnO$_2$(1200), Sn(12)Mo5Ni3, and Sn(6)Mo5Ni3 sensors at a H$_2$S concentration of 1 ppm and 350 °C. The response of the SnO$_2$(1200) sensor decreased gradually over multiple detection and recovery tests. On the other hand, the Sn(12)Mo5Ni3 sensor maintained its response over multiple tests without deactivation. The response of the Sn(12)Mo5Ni3 sensor was approximately double that of the Sn(6)Mo5Ni3 sensor.

Figure 8. Repeatabilities of the (a) SnO$_2$(1200); (b) Sn(12)Mo5Ni3; and (c) Sn(6)MoNi3 sensors.
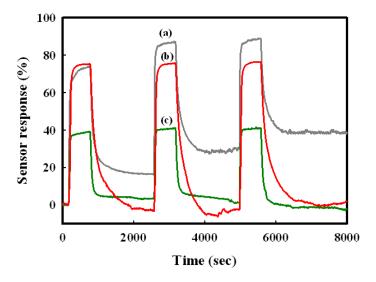

Figure 9 shows XRD patterns of Sn(6)Mo5Ni3 and Sn(12)Mo5Ni3 materials. Their XRD patterns showed MoO$_3$ (JCPDS No. 89-7112), NiO (JCPDS No. 89-7390) and SnO$_2$ (JCPDS No. 88-0287) phases. The diffraction peaks of these two materials were similar, as shown in Figure 9(a,b), which suggests that the observed enhancement in sensor response cannot be explained by structural differences alone. SEM images of the Sn(6)Mo5Ni3 and Sn(12)Mo5Ni3 sensors were observed at ×50 K and these results were shown in Figure 10. There is no change in the morphologies of those sensors as compared with the SnO$_2$(600) and SnO$_2$(1200) sensors. Table 3 lists the textural properties of the Sn(6)Mo5Ni3 and Sn(12)Mo5Ni3 materials determined by Hg porosimetry. The mean pore diameter of Sn(12)Mo5Ni3 was approximately double that of Sn(6)Mo5Ni (Table 3). This means that

the pore size of SnO_2 and the promoter play important roles in the sensor response to H_2S. Based on these results, we believe that it is possible to prepare an excellent SnO_2-based sensor for the detection of H_2S at concentrations of < 1 ppm with a high sensor response and excellent recovery properties using SnO_2 with a large pore size, in conjunction with NiO and MoO_3 promoters.

Figure 9. XRD patterns of the (**a**) Sn(6)Mo5Ni3 and (**b**) Sn(12)Mo5Ni3 materials; (◆) SnO_2, (nO MoO_3, and (nd NiO.
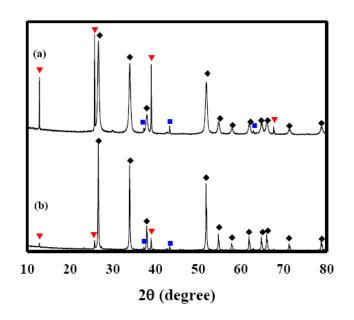

Figure 10. SEM images of the (**a**) Sn(6)Mo5Ni3 and (**b**) Sn(12)Mo5Ni3 sensors.
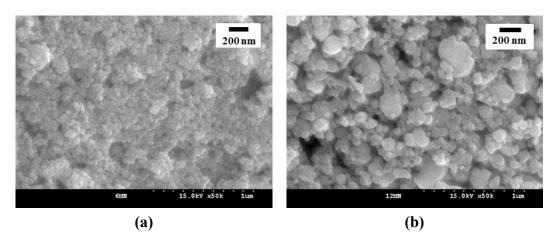

(**a**)   (**b**)

Table 3. Textural properties of the Sn(6)Mo5Ni3 and Sn(12)Mo5Ni3 by Hg porosimetry.

SnO_2 Materials	Surface Area (m^2/g)	Pore Volume (cm^3/g)	Average Pore Diameter (nm)
Sn(6)Mo5Ni3	11.8	0.5197	175.6
Sn(12)Mo5Ni3	4.7	0.4019	338.6

4. Conclusions

A new large pore size SnO_2-based thick-film gas sensor promoted with MoO_3 and NiO [Sn(12)Mo5Ni3] was developed for the detection of H_2S at 350 °C. This sensor exhibited 100%

recovery at 350 °C and a maximum sensor response of 75%, and maintained a sensor response of 75% over many operating cycles without deactivation at a H_2S concentration of 1 ppm and 350 °C. In addition, its response increased almost linearly between 0.25 and 1 ppm. Furthermore, the sensor exhibited a high response (59%) at a H_2S concentration of only 0.25 ppm. In particular, the Sn(12)Mo5Ni3 sensor exhibited double the response of the corresponding Sn(6)Mo5Ni3 sensor, which was prepared by adding MoO_3 and NiO to SnO_2 calcined at 600 °C. These results are explained by the promoter effects of MoO_3 and NiO, and the diffusion effects associated with a large SnO_2 pore size.

Acknowledgments

References

1. Hwang, I.S.; Choi, J.K.; Kim, S.J.; Dong, K.Y.; Kwon, J.H.; Ju, B.K.; Lee, J.H. Enhanced H_2S sensing characteristics of SnO_2 nanowires functionalized with CuO. *Sens. Actuators B* **2009**, *142*, 105–110.
2. Kim, S.Y.; Lee, S.C.; Hwang, B.W.; Lee, W.S.; Jung, S.Y.; Lee, D.D.; Kim, J.C. New SnO_2-based thick film gas sensor promoted with molybdenum and nickel oxides for H_2S detection. *J. Nanoelectron. Optoelectron.* **2011**, *6*, 293–296.
3. Jain, G.H.; Patil, L.A.; Wagh, M.S.; Patil, D.R.; Patil, S.A.; Amalnerkar, D.P. Surface modified $BaTiO_3$ thick film resistors as H_2S gas sensors. *Sens. Actuators B* **2006**, *117*, 159–165.
4. Yamazoe,; N. Matsushima, S.; Maekawa, T.; Tamaki, J.; Miura, N. Control of Pd-dispersion in SnO_2 based sensors. *Meas. Sci. Technol.* **1991**, *1*, 201–205.
5. Gong, J.; Chen, Q.; Lian, M.; Liu, N.; Stevenson, R.G.; Adamic, F. Micromachined nanocrystalline silver doped SnO_2 H_2S Sensor. *Sens. Actuators B* **2006**, *114*, 32149.
6. Lantto, V.; Romppainen, P. Response of some SnO_2 gas sensors to H_2S after quick cooling. *J. Electrochem. Soc.* **1988**, *135*, 255055556.
7. Liu, J.H.; Huang, X.J.; Ye, G.; Liu, W.; Jiao, Z.; Chao,W.L.; Zhou, Z.; BYu, Z.L. H_2S detection sensing characteristic of CuO/SnO_2 sensor. *Sensors* **2003**, *3*, 110–118.
8. Chowdhuri, A.; Gupta, V.; Sreenivas, K. Fast response H2S gas sensing characteristics with ultra-thin CuO islands on sputtered SnO_2. *Sens. Actuator B* **2003**, *93*,572–579.
9. Chowdhuri, A.; Gupta, V.; Sreenivas, K. Response speed of SnO_2-based H_2S gas sensors with CuO nanoparticles. *Appl. Phys. Lett.* **2004**, *84*, 1180–1182.
10. Kumar, R.; Khanna, A.; Tripathi, P.; Nandedkar, R.V.; Potdar, S.R.; Chaudhari, S.M.; Bhattti, S.S. $CuO.tha_2$ element as hydrogen sulfide gas sensor prepared by a sequential electron beam evaporation technique. *J. Appl. Phys.* **2003**, *36*, 237737381.
11. Katti, V.R.; Debnath, A.K.; Muthe, K.P.; Kaur, M.; Dua, A.K.; Gadkari, S.C.; Gupta, S.K.; Sahni, V.C. Mechanism of drifts in H_2S sensing properties of SnO_2:CuO composite thin film sensors prepared by thermal evaporation. *Sens. Actuators B* **2003**, *96*, 2454052.

12. Yuanda, W.; Maosong, T.; Xiuli, H.; Yushu, Z.; Guorui, D. Thin film sensors of SnO₂–nOsors,₂ sandwich structure to H₂S. *Sens. Actuators B* **2001**, *79*, 1878091.

13. Patil, L.A.; Patil, D.R. Heterocontact type CuO-modified SnO₂ sensor for the detection of a ppm level H₂S gas at room temperature. *Sens. Actuator B* **2006**, *120*, 316–323.

14. Wagh, M.S.; Patil, L.A.; Seth, T.; Amalnerkar, D.P. Surface cupricated SnO₂–ZnO thick film as a H₂S gas sensor. *Mater. Chem. Phys.* **2004**, *84*, 228–233.

15. Tsai, S.W.; Chiou, J.C. Improved crystalline structure and H₂S sensing performance of CuO-Au-SnO₂ thin film using SiO₂ additive concentration. *Sens. Actuators B* **2011**, *152*, 176–182.

16. Park, H.D.; Lee, D.D.; Lee, W.I.; Kim, J.M.; Kim, J.M. Sensitivity of SnO₂-based thick-film devices to CH₃CN. *Sensor. Meter.* **1994**, *5*, 209–220.

17. Liu, H.; Gong, S.P.; Hu, Y.X.; Liu, J.Q.; Zhou, D.X. Properties and mechanism study of SnO₂ nanocrystals for H₂S thick-film sensors. *Sens. Actuator B* **2009**, *140*, 190–195.

18. Brunol, E.; Berger, F.; Fromm, M.; Planade, R. Detection of dimethyl methylphosphonate (DMMP) by tin dioxide-based gas sensor: Response curve and understanding of the reactional mechanism. *Sens. Actuator B* **2006**, *120*, 35–41.

19. Berger, F.; Brunol, E.; Planade, R.; Chambaudet, A. Detection of DEMP vapors using SnO₂-based gas sensors: Understanding of the chemical reactional mechanism. *Thin Solid Films* **2003**, *436*, 136.

20. Choi, N J.; Lee, Y.S.; Kwak, J.H.; Park, J.S.; Park, K.B.; Shin, K.S.; Park, H.D.; Kim, J.C.; Huh, J.S.; Lee, D.D. Classification of chemical warfare agents using thick film gas sensor array. *Sens. Actuators B* **2005**, *108*, 298–304.

21. Kim, J.C.; Jun, H.K.; Huh, J.S.; Lee, D.D. Tin oxide-based methane gas sensor promoted by alumina-supported Pd catalyst. *Sens. Actuators B* **1997**, *45*, 271–277.

22. Lee, W.S.; Lee, S.C.; Lee, S.J.; Lee, D.D.; Huh., J.S.; Jun, H.K.; Kim, J.C. The sensing behavior of SnO₂-based thick-film gas sensors at a low concentration of chemical agent simulants. *Sens. Actuators B. Chem.* **2005**, *108*, 148–153.

23. Lee, W.S.; Choi, H.Y.; Lee, S.C.; Lee, S.J.; Lee, D.D.; Huh, J.J.; Kim, J.C. Recoverable SnO₂-based sensors promoted with MoO₃ and Sb₂O₃ for the detection of DMMP. *Rare Met. Mater. Eng.* **2006**, *35*, 155–156.

24. Lee, S.C.; Hwang, B.W.; Lee, S.J.; Choi, H.Y.; Kim, S.Y.; Jung, S.Y.; Ragupathy, D.; Lee, D.D.; Kim, J.C. A novel tin oxide-based recoverable thick film SO₂ gas sensor promoted with magnesium and vanadium oxides. *Sens. Actuators B* **2011**, *160*, 1328–1334.

25. Lee, S.C.; Kim, S.Y.; Lee, W.S.; Jung, S.Y.; Hwang, B.W.; Ragupathy, D.; Lee, D.D.; Lee, S.Y.; Kim, J.C. Effects of textural properties on the response of a SnO₂-based gas sensor for the detection of chemical warfare agents. *Sensors* **2011**, *11*, 6893–6904.

26. Lee, S.C.; Choi, H.Y.; Lee, S.J.; Lee, W.S.; Huh, J.S.; Lee, D.D.; Kim, J.C. The development of SnO₂-based recoverable gas sensors for the detection of DMMP. *Sens. Actuators B* **2009**, *137*, 239–245.

27. Lee, S.C.; Choi, H.Y.; Lee, S.J.; Lee, W.S.; Huh, J.S.; Lee, D.D.; Kim, J.C. Novel SnO₂-based gas sensors promoted with metal oxides for the detection of dichloromethane. *Sens. Actuators B* **2009**, *138*, 446–452.

28. Lee, S.C.; Choi, H.Y.; Lee, W.S.; Lee, S.J.; Ragupathy, D.; Lee, D.D.; Kim, J.C. Improvement of recovery of SnO_2-based thick film gas sensors for dimethyl methylphosphonate (DMMP) detection. *Sens. Lett.* **2011**, *9*, 101–105.

29. Lu, C,H.; Yeh, C.H. Influence of hydrothermal conditions on the morphology and particle size of zinc oxide powder. *Ceram. Int.* **2000**, *26*, 351–357.

30. Chena,Y.F.; Lee, C.Y.; Yeng, M.Y., Chiu. H.T. The effect of calcination temperature on the crystallinity of TiO_2 nanopowders. *J. Cryst. Growth* **2003**, *247*, 363–370.